



HAL
open science

A Stochastic Multi-Agent Approach for Medical-Image Segmentation: Application to Tumor Segmentation in Brain MR Images

Mohamed Bennai, Zahia Guessoum, Smaine Mazouzi, Stéphane Cormier,
Mohamed Mezghiche

► **To cite this version:**

Mohamed Bennai, Zahia Guessoum, Smaine Mazouzi, Stéphane Cormier, Mohamed Mezghiche. A Stochastic Multi-Agent Approach for Medical-Image Segmentation: Application to Tumor Segmentation in Brain MR Images. *Artificial Intelligence in Medicine*, 2020, 110, pp.101980. 10.1016/j.artmed.2020.101980 . hal-03740060

HAL Id: hal-03740060

<https://hal.science/hal-03740060>

Submitted on 21 Nov 2022

HAL is a multi-disciplinary open access archive for the deposit and dissemination of scientific research documents, whether they are published or not. The documents may come from teaching and research institutions in France or abroad, or from public or private research centers.

L'archive ouverte pluridisciplinaire **HAL**, est destinée au dépôt et à la diffusion de documents scientifiques de niveau recherche, publiés ou non, émanant des établissements d'enseignement et de recherche français ou étrangers, des laboratoires publics ou privés.



Distributed under a Creative Commons Attribution - NonCommercial 4.0 International License

A Stochastic Multi-Agent Approach for Medical-Image Segmentation: Application to Tumor Segmentation in Brain MR Images

Mohamed T. Bennai^{a,b}, Zahia Guessoum^{b,c,*}, Smaine Mazouzi^d, Stéphane Cormier^b, Mohamed Mezghiche^a

^a*LIMOSE Laboratory, Faculty of Sciences, University of M'hamed Bougara of Boumerdes, Avenue de l'indépendance, 35000, Boumerdes, Algeria*

^b*Université de Reims Champagne Ardenne, CReSTIC EA 3804, 51097 Reims, France*

^c*Sorbonne Université, LIP6 UMR7606, 75005 Paris, France*

^d*Dept. of Computer Science, Université 20 Août 1955, Skikda, Algeria*

Abstract

According to functional or anatomical modalities, medical imaging provides a visual representation of complex structures or activities in the human body. One of the most common processing methods applied to those images is segmentation, in which an image is divided into a set of regions of interest. Human anatomical complexity and medical image acquisition artifacts make segmentation of medical images very complex. Thus, several solutions have been proposed to automate image segmentation. However, most existing solutions use prior knowledge and/or require strong interaction with the user. In this paper, we propose a multi-agent approach for the segmentation of 3D medical images. This approach is based on a set of autonomous, interactive agents that use a modified region growing algorithm and cooperate to segment a 3D image. The first organization of agents allows region seed placement and region growing. In a second organization, agent interaction and collaboration allow segmentation refinement by merging the over-segmented regions. Experiments are conducted on magnetic resonance images of healthy and pathological brains. The obtained results are promising and demonstrate the efficiency of our method.

*Corresponding author

Email address: Zahia.Guessoum@univ-reims.fr (Zahia Guessoum)

Keywords: 3D Medical Images, Segmentation, Multi-Agent Systems, Region Growing, Region Merging

1. Introduction

Medical imaging plays an important role in medicine. It has generated significant research interest and imaging-based healthcare solutions. Medical image segmentation is one of the most challenging tasks in this field. It is a crucial non-invasive technique that can provide information regarding structures in the human body.

Several segmentation algorithms and methods have been developed. The proposed solutions include thresholding [1], region growing [2, 3], and more sophisticated computing methods, such as those using Markov random fields [4] and deformable models [5]. Most existing segmentation solutions [6, 7] are not democratized because they require user interaction and/or considerable computing time.

Recently, the research community has significantly improved the performance of medical image segmentation systems using advances in machine learning, particularly in deep learning [8, 9], which provides promising results. However, new concerns related to the learning process have been raised, such as the need to build large volumes of manually segmented data, time and energy required for learning, and risk of over-fitting. To prevent these problems, researchers are exploring the possibilities offered by multi-agent systems (MASs).

A MAS is composed of a population of software entities called agents, which are situated in an environment and capable of making autonomous decisions in this environment, to meet their local objectives and the global purpose of the system [10]. MASs provide a distributed and collective decision process that allows segmentation of medical images with flexibility, autonomy, and robustness. Thus, they have been used for medical image segmentation [11] during the prior decades. However, these approaches still suffer from several drawbacks, such as the excessive number of parameters and the need for user interaction. Moreover, most existing approaches have been designed for one type of image and cannot be easily reused for another type. Therefore, we propose a new multi-agent approach for medical image segmentation. This approach is based on a population of situated agents, which move, interact, and coordinate their actions in an image (agent envi-

ronment) to perform segmentation. This allows a novel distributed segmentation tool to be built for segmenting brain magnetic resonance (MR) images. Moreover, the method combines locality and stochasticity to overcome the intensity non-uniformity (INU) artifact. Locality is insured by using situated agents, where each agent processes a sub-region of the image using its specific parameters. Stochasticity is insured by the randomness of agents when they move within the image using a random walk search. The proposed approach relies on two steps without any user interaction.

- In the first step, a set of agents start partitioning voxels in the image into edge voxels and non-edge voxels based on the magnitude of the gradient between voxels.
- In the second step, another set of agents use the obtained voxel partition to detect and extract homogeneous regions in the image.

The aim of this study is to present the proposed approach and illustrate its effectiveness in segmenting medical images. The remainder of the paper is organized as follows. The context of this study and related research are described in Section 2. The proposed multi-agent approach is introduced in Section 3. Details regarding implementation and experimental results for both tissue segmentation and tumor detection in magnetic resonance imaging (MRI) are presented in Section 4. Finally, some perspectives and conclusions are offered in the last section.

2. Related Work

Automated medical image segmentation is very challenging due to the complexity of acquisition methods and the inherent artifacts in medical images. Several solutions have been proposed (see [12]). An overview of medical image segmentation challenges and related works are introduced in this section.

2.1. Medical Image Segmentation

Segmentation of functional or anatomical medical images provides information of interest about structures or activities in the human body. It helps radiologists and physicians visualize and study the anatomy of those structures. The obtained information is used for different purposes, such as

pathology diagnostics, pre-operative planning, image-guided surgical procedures, disease progress tracking, and treatment planning [13].

Accurate segmentation is vital in medical imaging, but ensuring accurate segmentation is difficult. The difficulty of segmenting such images comes from different factors including: 1) acquisition and sampling methods (e.g., CT scans and magnetic resonance images) generate noise, non-uniform intensity (at acquisition), and partial volume effect (at sampling); 2) the complexity of human anatomical structures; 3) the closeness in gray level of different soft tissues (low contrast) [12].

A wide range of medical image segmentation approaches has been introduced for segmenting different types of images for several pathologies. Those approaches use different techniques, such as thresholding [1], region growing [2, 3], Markov random fields [4], fuzzy and hard clustering [14, 15], and deformable models [5]. They often require pre-processing tasks to reduce noise and correct artifacts, and some require manual initialization [16].

Execution of these existing segmentation algorithms depends on the visual primitives that must be extracted, such as specific regions or contours. There are several literature reviews of the most recent approaches ([17, 18, 19]).

Gray level thresholding allows differentiation of various areas in an image, leading to segmentation. However, the presence of noise in medical images and intensity inhomogeneity within the tissue make the direct thresholding of gray levels inapplicable to medical image segmentation.

Moreover, region growing techniques suffer from the problem of seed selection. Without the use of prior knowledge, it is difficult to define a criterion to select a given voxel of the image as the starting point of the growing process. Some medical image segmentation systems have changed the initial region growing algorithm by introducing different enhancements. In [20], the authors define some criteria for growing algorithms to be independent of the seed regions and the order of region treatment. In the approach presented by [21], the contrast of a region is defined in terms of the gradient across its border. This definition provides significantly higher segmentation accuracy.

Voxel classification allows different regions corresponding to tissues of interest in the image to be obtained. Voxel classification methods are either statistical or fuzzy. The parameters of a statistical model are estimated either from a set of labeled data or using a given heuristic, such as expectation maximization. In both approaches, an estimator, such as maximum a posteriori (MAP), is used to calculate the most likely class to which the voxel belongs [22, 23]. The exploitation of local links between voxels via Markovian

models provides segmentation with higher accuracy [24, 25]. Classification methods are also used to analyze voxels in a medical image, with the fuzzy C-means (FCM) algorithm being the most popular [26, 27].

Manually segmented images are used in several new segmentation methods, such as Atlas methods [28]. Atlas methods allow radiometric and spatial knowledge to be represented in a given type of image. They were initially introduced in [29]. Although they have been very successful, different improvements and combinations with other methods have been proposed [30, 31].

Machine learning techniques are also used for classifying medical images as part of segmentation using a dataset of manually labeled images. Machine learning approaches are first trained on these manually labeled data, and segmentation is performed using the trained model. Many machine learning-based medical image segmentation approaches have been proposed in the literature, such as decision tree [32], support vector machine [33], random forest [34], and more recently, deep learning methods [35]. Similar to machine learning approaches, medical image segmentation techniques using manually annotated data offer outstanding results particularly when deep learning methods are used. However, several challenges hamper their democratization, such as the lack of manually labeled medical images, class imbalance inside training datasets, and overfitting [35].

Despite the advances made in the last few years within the medical imaging research community, correct identification and segmentation of all tissues present in a medical image remains a complex task, and its automation remains a challenge. Rather than attempting to segment all the tissues present in a medical image, researchers have focused on identifying and isolating pathological tissues (e.g., detection of Alzheimer lesions or tumors), providing valuable information for medical staff. Tumor segmentation is one of the most active areas in the medical image segmentation field, and many studies have been published on tumor segmentation in MR brain images. A brief overview of these earlier studies is presented in the next section.

2.2. Tumor Segmentation

MRI is a non-invasive in vivo imaging technique that uses a radio frequency magnetic field to excite target tissues, and an image is generated from the magnetic field produced by certain tissues at different frequencies [36]. MRI is commonly used for brain tumor imaging and diagnosis. Using different MRI sequences (also known as modalities), medical professionals can analyze images and collect crucial structural information regarding the

condition of brain tissues to detect possible brain tumors and, in such cases, monitor evolution of the disease. This analysis is mainly conducted by segmenting MR images with the aim of identifying the tumor from the rest of the tissues. Manual segmentation of a brain tumor is a time-consuming and challenging task, even for domain experts. Therefore, the development of a technique for automatic segmentation of brain tumors in MRI is a major challenge as it accelerates and improves patient treatment by reducing practitioner workloads. However, automatically segmenting a brain tumor is a complicated task due to the variability in tumor shapes, textures, sizes, and locations; image variations due to intrinsic differences in acquisition protocols and devices; and MRI well-known artefacts (i.e., noise, low contrast, and partial volume effect).

During the prior decades, many methods have been proposed for brain tumor segmentation in MRI. Classical segmentation methods were used in early studies to extract tumors in MR brain images. They have allowed exploration of this application domain, despite their limitations. New approaches use a combination of several existing techniques in the same system with the intent of improving the segmentation quality by putting these techniques in competition. Some of those approaches are reviewed in [37, 38, 39, 40, 41]. Another type of approach relies on machine learning. Instead of using different algorithms to isolate the tumor from the rest of the image, machine learning techniques use training datasets to generate models based on pattern matching and similarities. Those techniques have generated considerable interest in medical image segmentation and tumor segmentation in brain MRI.

Several machine learning approaches have been proposed and can be classified into two main categories: generative models and discriminative models. The latter have emerged from democratization of deep learning and convolutional neuronal networks (CNN) [42]. Unlike traditional classification methods, where images with manually tagged features are used for training, CNNs automatically learn complex representative features directly from the data itself. Research on CNN-based brain tumor segmentation mainly focuses on network architecture design rather than image processing to extract features [36]. This focus is motivated by the results obtained with these methods using available segmentation benchmarks. As an example, during the last Brain Tumor Segmentation (BraTS) challenge [43], a well-known dataset and challenge for MRI brain tumors segmentation, first place was exclusively won using deep learning-based approaches. Despite their effectiveness in dealing with benchmarks, deep learning-based approaches suffer from the following

limitations [44]:

- **Lack of training datasets:** Training deep networks with imbalanced data can produce biased models [44]. Thus, with the brain tumor segmentation (BraTS) dataset, where all provided images (training, validation, and testing) contain tumors, deep learning-based approaches offer substantial results for tumor segmentation. Nevertheless, these results do not ensure the accuracy of deep learning approaches when dealing with a healthy brain or tissues affected by a disorder unrelated to a tumor.
- **Lack of appropriately tagged data:** Deep learning approaches are designed to learn from a vast amount of training data, while the set of available manually segmented medical images is limited.
- **Overfitting:** An excessive training phase applied to a highly specific dataset may lead to a model that is suitable to these data but cannot be generalized to other data.

Most of the approaches listed above employ a monolithic, sequential, centralized process to perform tumor segmentation [45]. Furthermore, they use a unidirectional execution, where backtracking is impossible during the segmentation process. Thus, these approaches ignore other segmentation choices that can be more significant than the considered one. Some novel approaches for increasing the efficiency of a segmentation system, regardless of the used classification technique being used, have been proposed. They are based on a collaborative problem-solving paradigm called MASs. Those studies are reviewed in the next section.

2.3. Multi-Agent Segmentation Approaches

MASs have been successfully used for automated imaging-based diagnostics [11], where image segmentation is a critical step. Several multi-agent approaches have been proposed for medical image segmentation. We distinguish these into two categories. In the first category, each agent encapsulates one of the various existing methods (e.g., edge detection [46], region detection [47], or meta heuristic [48]). A MAS aims to improve segmentation using different mechanisms such as distribution and information diffusion. The second category aims to use MASs by using the underlying mechanisms. The solutions in this category rely on social coordination mechanisms, such

as ant colonies and social spider colonies [49]. For instance, Djemame et al. [50] used self-organization and adaptation of social spiders in a MAS to extract homogeneous regions in an image. Liu and al.[51] used agents with unicellular living-beings behavior to extract brain structures in a computed tomography (CT) image. Richard et al. [52] use cooperative and interactive behaviors to respectively distribute the classification task and propagate information among agents to segment medical images.

The region growing method is well suited for multi-agent medical image segmentation systems in the aforementioned categories [53]. This success is due to the robustness, rapidity, and simplicity of the region growing algorithm [54]. Multi-agent exploitation of the region growing algorithm also permits the drawbacks of seed selection and region characteristics definition to be overcome. Some systems use this technique to label pixels from a set of known classes in sub-regions within an image; such a technique was used with brain MRI [55] and CT image scans [56]. Other multi-agent approaches combine region growing and other segmentation methods, such as the fuzzy C-mean method for segmenting brain MR images [57], region fusion in the same type of image, or region fusion for micro aneurysm detection in fundus images [58].

Existing multi-agent approaches have been successfully used for image segmentation. Most of those multi-agent approaches are either based on centralized agents or a set of agents encapsulating segmentation algorithms and acting on portions of the image. The second category of approaches uses agents to distribute the segmentation process, but most of those approaches do not use a coordination mechanism. So, they do not exploit the full advantages of MASs, such as decision distribution, coordination, and interaction.

2.4. Discussion

In the current section, we reviewed several interesting and innovative segmentation approaches. Most of those approaches provide promising results. However, they suffer from one or more of the following drawbacks [59]:

- Most of those approaches require user intervention for defining parameters, thresholds, or where segmentation starts.
- The best approaches, in terms of segmentation accuracy, require a long time (several hours in some studies). Thus, they cannot be used by physicians in real time.

- Learning-based approaches require a considerable amount of manually segmented 3D MRI images, which is hard to find or to produce.

Furthermore, and to overcome computational complexity, especially for 3D images, several methods proceed by partitioning the volume of voxels into subsets, primarily into sub-cubic volumes [52] or slices [51]. Such techniques reduce processing complexity and allow classical operators developed for 2D images to be used. However, interaction among neighboring voxels that belong to adjacent sub-volumes are omitted, resulting in information loss, and concerned voxels can be incorrectly categorized.

To overcome some of these drawbacks, we developed an adaptive multi-agent approach for tumor segmentation in 3D MRI of the brain. The proposed approach is described in the following section.

3. MAMES: A Multi-Agent approach For MEDical image Segmentation

Our multi-agent approach for medical image segmentation (MAMES) is introduced in this section. MAMES relies on an evolution of the multi-agent approach presented in [59]. A population of rationally situated agents is launched to perform image segmentation. The agents are situated in an environment that represents the 3D image. Each voxel in the 3D image contains the gray level intensity and the local gradient vector. The latter is obtained by applying a 3D Sobel filter to the processed image (see [60] for more details). The 3D version of the Sobel filter allows edge voxels to be detected in 3D images.

Agents first classify image voxels into two categories: region and non-region voxels. This classification is used to select seeds for the next region growing step. Starting from the selected seeds, agents initiate then region growing by iteratively assimilating neighboring voxels. In the last step, the agents interact with each other to merge homogeneous neighboring regions when needed. The following sections describe these two tasks (partition and region growing) and show how they are performed according to different agent behaviors.

3.1. Voxel Partitioning

Fig.1 illustrates how agents are distributed in the 3D volume. At each time step, the system considers slices from each orthogonal plane in the image

(axial, coronal, and sagittal). Each slice represents a two-dimensional gray level image in that series, where voxels are processed as pixels. Then, agents are uniformly dispersed in each slice, as demonstrated in Fig.1. Thus, an area of voxels is assigned to each agent. This area represents the set of voxels to be processed by the agent after activation, with the aim of identifying pixels along contours in those of regions.

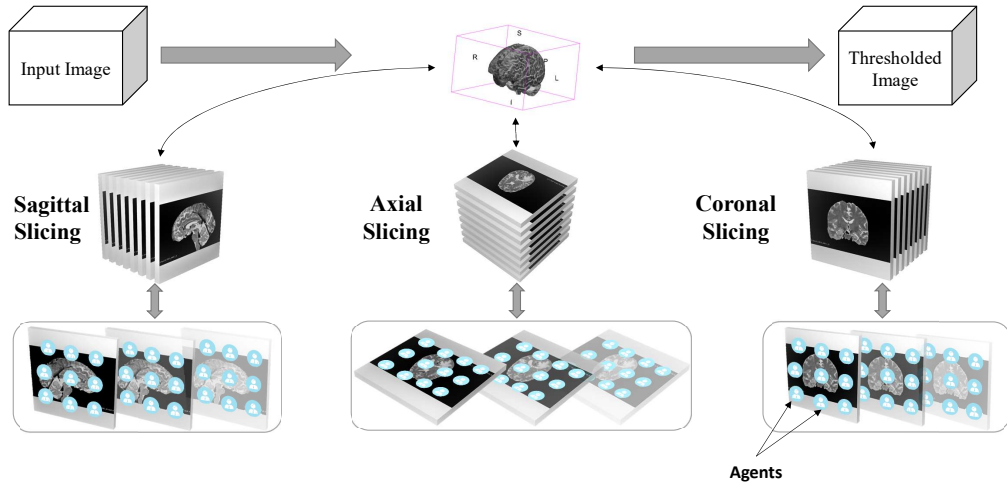


Fig. 1: Agent distribution during thresholding

After activation, an agent analyzes the gray magnitude (GD) in its local area. The agent uses a classical k -means clustering algorithm to perform classification of those voxels according to their gradient magnitude, where $k = 2$ (the number of desired classes). Two classes are thus considered (edge voxel or inside-region voxel):

- Class (C^1): voxels with high magnitude gradient (edge voxels and their neighbors),
- Class (C^2): voxels with low magnitude gradient (voxels inside regions).

Thus, each voxel is thresholded three times (along the three planes) to maximize the chance of detecting neighboring pixels. Also, a voxel is finally assigned to (C^2) if it was classified accordingly in the three planes. Meanwhile, a voxel is assigned to (C^1) if it was classified accordingly just by one agent (one plane).

The set of the voxels labeled as belonging to borders (C^1) with the k -means algorithm is discarded from the set of area voxels inside the agent processing zone. The remaining cluster of region voxels (C^2) is either composed of continuously adjoining voxels or partitioned into several sub-parts. In the latter case, the agent creates a new agent for each contiguous part of voxels, then it disappears.

At the end of this step, each new agent has its own set of C^2 voxels. This set may be composed of all the voxel inside the agent's area, or a sub-region after discarding the edge voxels and partitioning the region voxels in contiguous sub-regions.

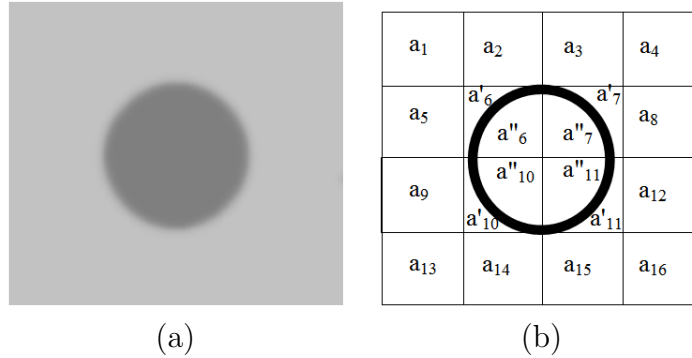


Fig. 2: Sub-area partitioning for region seed selection: (a) raw image, and (b) partitioned image

Fig.2 shows an image composed of two homogeneous regions separated by a fuzzy outline (circle). Agents a_1, \dots, a_{16} are uniformly scattered on the image. Any agent having a non-homogeneous area decomposes its set of voxels into two homogeneous partitions:

- C^2 : belonging to the inside of the regions,
- C^1 : forming the contours between regions and their respective neighbors (thick circle in Fig.2), represented by agents a_6, a_7, a_{10} , and a_{11} .

Each of these agents creates an agent for each partition of contiguous voxels. For example, agent a_6 creates agents a'_6 and a''_6 , then it self-destructs. In the given example, this results in a population of 20 agents following the creation of 8 agents and destruction of 4 agents. This process produces two sub-graphs corresponding to the two homogeneous regions in the image. This result consists respectively in the sub-graphs $\{a_1, a_2, a_3, a_4, a_5, a'_6, a'_7, a_8, a_9, a'_{10}, a'_{11}, a_{12}, a_{13}, a_{14}, a_{15}, a_{16}\}$ and $\{a''_6, a''_7, a''_{10}, a''_{11}\}$.

3.2. Seed Selection

At the end of the partitioning task, the agents are connected in an adjacency graph, where two agents are adjacent if there is a linear sequence of C^2 voxels connecting them in the image. Therefore, for each connected sub-graph, the agent with the highest number of adjacent peers is selected to start region growing from its seed voxel. With the graph partitioning results presented in Fig.2, only two agents (one for each sub-graph) will be in charge of region growing. Considering the first region (R_1), only one agent will be randomly chosen among agents $a'_6, a'_7, a'_{10}, anda'_{11}$, and its position will become the seed of this region because each region is adjacent to three others. Similarly, an agent will be selected among agents $a''_6, a''_7, a''_{10}, anda''_{11}$ as each agent is adjacent to 2 others, regarding the second region (R_2).

3.3. Region Growing

The remaining population of agents allows the extraction of the regions composing the image. Those agents use a modified version of the region growing method (proposed in [61] and used in [59]) and were adapted for 3D images. An agent starts growing its region from its seed voxel (set in the previous stage) in two phases: initial and final region growing.

3.3.1. Initial Region Growing

This first phase allows the characteristics of the region to be computed. Starting from the seed voxel, each agent uses a random walk and adds to its initial region R_{init} any voxel P classified as C^2 and with a gray level close to the gray level of the growing region. In other words, a voxel P is added to the initial region R_{init} during the random walk if it satisfies the following conditions:

$$G(P) \in [T_{upper}, T_{lower}] \quad \bigwedge \quad P \in C^2 \quad (1)$$

$$\text{with} \quad T_{upper} = Md(R_{init}) + ((\sigma_u(R_{init}) \times w) + c(R_{init})) \quad (2)$$

$$\text{and} \quad T_{lower} = Md(R_{init}) - ((\sigma_l(R_{init}) \times w) + c(R_{init})) \quad (3)$$

where $G(P)$ is the gray level of P , C^2 is the class of region voxels, $Md(R_{init})$ is the median gray level value of R_{init} , $\sigma_l(R_{init})$ and $\sigma_u(R_{init})$ are respectively the lower and upper standard derivations of R_{init} , w and $c(R_{init})$ allows the homogeneity of R_{init} to be adjusted.

The first condition in Eq.(1) uses T_{upper} and T_{lower} proposed in [61]. We add the second term to account for the intensity and prevent the agent from crossing a contour, which would cause the agent to overflow into another region during this initial step of region growing and exploration. The agent stops its random walk when it performs several walks without adding any voxels or the execution time limit is reached. In both cases, the agent goes back to the initial voxel (seed) and starts the next step.

Use of a classical recursive random walk for voxel browsing and region growing allows diversification of voxels during the initial region growing. The set of voxels reached by a random walk does not necessarily form a small region around the seed voxel. However, when those voxels have the same main characteristics, they are representative of the entire region. Additionally, the random walk ensures voxels in the initial region kernel are contiguous; they are obtained by random walking within the neighborhood. Such a process ensures the continuity, the compactness, and the uniformity of the browsed set of voxels. Besides, the agent uses this set to compute the explored region’s statistics when finishing its exploration.

Algorithm 1 presents our 3D version of the random walk algorithm in spherical coordinates. *MaxTime* is the number of steps to be walked by an agent before stopping and then computing the initial region features. The spherical coordinates x , y , and z are expressed as follows: $x = r \times \cos(\theta) \times \sin(\phi)$, $y = r \times \sin(\theta) \times \sin(\phi)$, and $z = r \times \cos(\theta)$ with $r = \sqrt{x^2 + y^2 + z^2}$. For one step within the unit cube ($dr = (1, 1, 1)$), an agent computes its direction in the horizontal plane in terms of θ and with respect to the z axis in terms of ϕ . The three components of one step are then expressed as follows: $dx = dr \times \cos(\theta) \times \sin(\phi)$, $dy = dr \times \sin(\theta) \times \sin(\phi)$, and $dz = dr \times \cos(\theta)$, where $dr = \sqrt{1^2 + 1^2 + 1^2} = \sqrt{3}$. In the implementation, θ and ϕ are calculated according to the execution time; therefore, they vary strongly at the beginning of the move, allowing the agent to browse most of the voxels around the seed. The increase of the execution time leads to a reduction in θ and ϕ fluctuations, causing the agent to explore regions that are increasingly distant from its seed pixel (Fig.3).

3.3.2. Final Region Growing

In this step, and to finalize region growing, each agent uses the region statistics computed in the previous phase. These statistics consist of the mean and standard-derivation ($E_{R_{init}}(G), \sigma(R_{init})$) of the voxel gray level browsed during the random walk. They are used to evaluate the predicate of

Algorithm 1 Method *3D Random Walk*(*int* x^a, y^a, z^a)

```
 $path \leftarrow \{(x^a, y^a, z^a)\}$   
 $Time \leftarrow MaxTime$   
while  $Time > 0$  do  
   $\theta \leftarrow 2\pi \times random \times Time/MaxTime$   
   $\phi \leftarrow \pi \times random \times Time/MaxTime$   
   $dx \leftarrow \sqrt{3} \times \cos(\theta) \times \sin(\phi)$   
   $dy \leftarrow \sqrt{3} \times \sin(\theta) \times \sin(\phi)$   
   $dz \leftarrow \sqrt{3} \times \cos(\phi)$   
   $x^a \leftarrow x^a + dx$   
   $y^a \leftarrow y^a + dy$   
   $z^a \leftarrow z^a + dz$   
   $path \leftarrow path + \{(x^a, y^a, z^a)\}$   
   $Time - -$   
end while
```

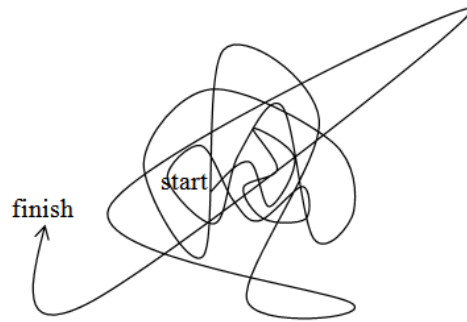


Fig. 3: Path produced by a random walk where the agent progressively enlarges its scope around its initial position

voxel assimilation (Eq.(4)) during the remaining final region growing phase.

$$Predicate(P) = \begin{cases} true & \text{if } G(P) \in [E_{R_{init}}(G) \pm (\sigma(R_{init}) \times \alpha)] \\ false & \text{otherwise} \end{cases} \quad (4)$$

Starting from the seed voxel, the agent extracts its final region using the computed mean, standard deviation, and α (an assimilation tolerance parameter) according to their prior classification (C^1 or C^2). At each step, the agent browses the set of contour voxels surrounding its region. It then assimilates all voxels that satisfy the assimilation predicate. This growing process is repeated while there are absorbable non-allocated voxels (voxels that satisfy the region assimilation predicate) surrounding the current region.

3.4. Merging

The previous phases allow agents to detect regions, where an agent is associated with each region. In this new phase, the agents use a region neighborhood concept to merge the already-detected regions. Indeed, as an intensity non-uniformity correction has not been performed, a homogeneous region may be split into several regions obtained by region growing starting from their own seed. Two regions are considered neighbors if they have adjacent borders. Thus, each agent aims to expand its region by integrating other regions from its neighbors. However, merging requires the approval of the neighboring agents.

A high number of merging combinations is to be considered according to the region's characteristics. To address such merging problem, we propose to endow the agents with 1) an interaction protocol that is based on the contract net protocol (CNP), and 2) a decision strategy that is based on a social welfare (see subsection 3.4.2) [62].

3.4.1. Interaction Protocol

To communicate with their respective neighbors, the agents use the CNP [63] to select which agents will be attached. According to this selection, agents update their neighborhood and restart looking for other agents to attach. The process is repeated until no more agents can be attached after a timeout. The main steps of this communication protocol are as follows (Fig.4):

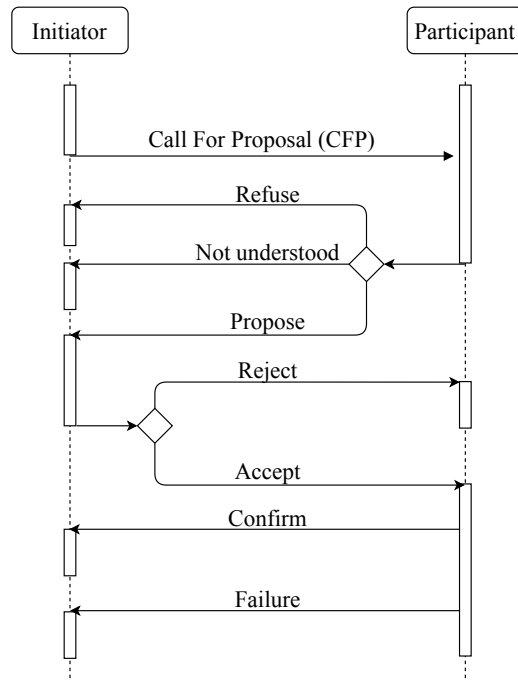


Fig. 4: Contract net protocol

- **CFP:** First, each agent computes its standard deviation and sends an attachment request with a “call for proposal” message with this value and a timeout to all its neighbors.
- **Refuse/Propose:** When receiving an attachment request, an agent analyzes the standard derivation of its region when merging with that of the participant. If this merging increases its standard deviation, it then sends a propose message; otherwise, it sends a refuse message to the sender.
- **Accept/Reject:** After the time out, the initiator analyzes the proposals. It selects the proposal that satisfies the social welfare (see Section 3.4.2). The agent then sends an accept message to the associated agent, which will be attached, and a reject message is sent to the other agents.
- **Failure/Confirm:** When receiving an accept message, an agent sends a confirm message if it has not accepted another attachment request; otherwise a failure message is sent.

- **Attachment:** When receiving a confirm message, the agent attaches the participant and waits for the next iteration.

Each agent repeats the process while it has proposals from its neighbors. Otherwise, the agents consider the current solution to be optimal.

3.4.2. Merging decision

When receiving several proposals for merge requests, an agent A (managing region R) can use several strategies to select one of those proposals. This individual decision has an important impact on global image segmentation. So, an important question is, what is the best individual strategy that generates efficient segmentation? Furthermore, how should efficient segmentation be characterized given the individual objectives? This question is addressed in social choice theory (SCT) [64],[65] and welfare engineering [66].

In SCT, a society of agents is considered, where each agent expresses preferences over a set of alternatives. This theory studies the so-called “social welfare functions.” Such functions aggregate individual preferences to produce a social preference over the alternatives. Each agent can thus select a strategy that optimizes the social welfare function.

Social welfare functions are analyzed w.r.t. the utilitarian/egalitarian axes. In this study, we focus on egalitarian welfare, which maximizes the welfare of a less satisfied agent [67] (Eq.5). Agent welfare is defined as the standard deviation of the voxel intensities within its region. Therefore, when receiving one or several proposals to merge, an agent A (managing region R) chooses to merge with agent A_j (managing region R_j) that satisfies:

$$\sigma(R \cup R_j) = \min_{R_i \in Adj(R)} (\sigma(R_1 \cup R_i)) \quad (5)$$

where $Adj(R)$ represents the set of agents adjacent to A and $\sigma(R)$ is the standard-deviation of region R .

Region merging is the final phase of our approach. Thus, the image segmentation results contain a set of homogeneous regions, regardless of what they may represent.

To measure the efficiency of MAMES and ensure its robustness, we performed experiments with healthy and pathological brain MR images. Implementation and experimental results are described in the following section.

4. Experiments and Results

This section provides an overview of our implementation, and the experimental results are introduced and analyzed. These experiments were performed on a computer equipped with an Intel I7-6500U processor (2.5 GHz frequency, two physical cores, four threads) and 16 GB RAM.

4.1. Implementation

Our MAMES experiments were implemented using C# and MS Net. The latter allows medical images to be easily segmented with acceptable accuracy and execution time. All entities used in the system were implemented as C# classes, including the agents. The framework is developed as a desktop application with a simple and convivial interface (Fig.5). It can process both standard 2D and 3D image formats. It can also extract 2D slices from image volumes. The framework offers the following features:

- Visualizing 2D images;
- Visualizing 3D volumes and extracting 2D slices for segmentation;
- Segmenting an image with MAMES;
- Viewing classification results obtained after distributed thresholding (first step);
- Viewing regions detected by the system;
- Viewing the characteristics (size, average gray level, standard derivation) of the detected regions;
- Viewing the detected contours.

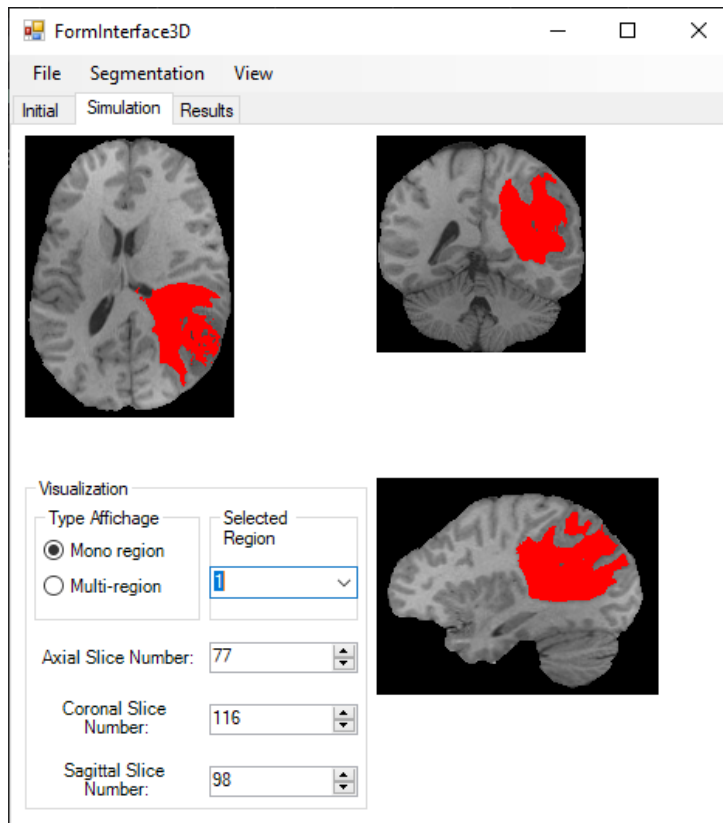


Fig. 5: MAMES interface

To evaluate the efficiency of our multi-agent image segmentation approach and to insure its robustness, we conducted multiple experiments with different types of brain MR images.

The evaluation metric was the Dice similarity coefficient [68], also known as κ coefficient (kappa). This coefficient is commonly used in medical image processing to evaluate the performance of segmentation algorithms by comparing the obtained results with predefined reference information. It is calculated using the following formula [59]:

$$Dice = \frac{2 \times TP}{2 \times TP + FP + FN} \quad (6)$$

where TP , FP , and FN are the true positive, false positive, and false negative rates of pixel labeling, respectively. The value of the Dice coefficient sufficiently expresses segmentation accuracy.

4.2. Experimental Results on 2D MR Phantom Images

The first series of experiments was performed on brain MRI 2D phantom image slices extracted from 3D brain MR images. Those images were generated from the BrainWeb platform, a phantom database provided by the McConnell Brain Imaging Center at Montreal Neurological Institute (<https://brainweb.bic.mni.mcgill.ca/brainweb/>) [69].

According to Collins [69], simulated phantom images are an effective tool for validating the results of a segmentation algorithm. They also permit a comparison with results obtained from other published methods. Moreover, we chose the simulated images generated by BrainWeb because this tool allows the efficiency and robustness of MAMES to be evaluated despite the presence of image artifacts, such as noise and INU, in a quantitative evaluation. Consequently, we used MR Simulator (MRISIM) to generate realistic brain MR images with the T1 modality for our experiments.

MRISIM allows the user to generate a brain MR image by combining three different modalities ((T1-, T2-, and Proton-Density), five slice thickness values, six levels of noise (0%, 1%, 3%, 5%, 7%, and 9%), and three INU levels. For our tests, we used the T1 modality and 1 mm thickness as fixed values, and we varied the INU (0%, 20%, and 40%) and noise (0%, 1%, 3%, 5%, 7%, and 9%), giving a total of 18 MR images. Moreover, each volume is stored as a 3D matrix of $181 \times 217 \times 181$ voxels. The segmentation results are summarized in Table 1 and illustrated in Fig.6.

INU level	Noise level					
	0%	1%	3%	5%	7%	9%
0%	90%	91%	93%	95%	94%	91%
20%	92%	91%	94%	95%	93%	87%
40%	89%	91%	91%	89%	86%	85%

Table 1: Dice coefficient for white matter extraction with different noise and INU levels

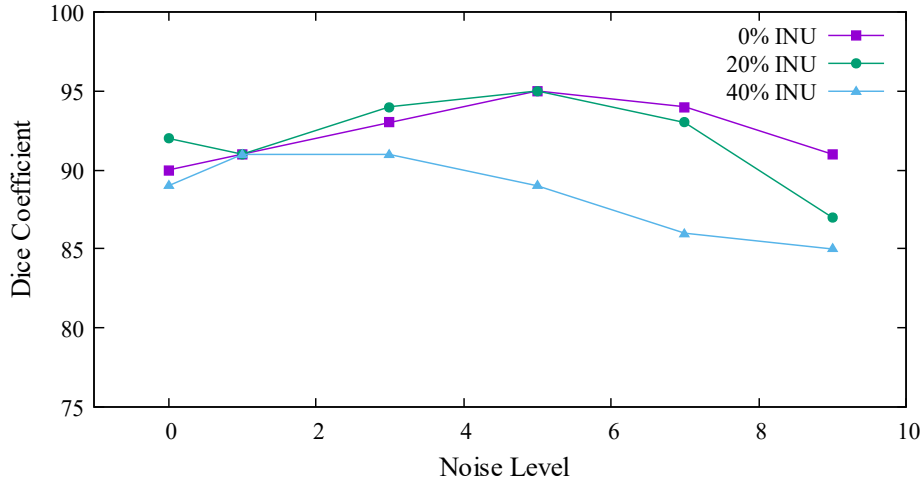


Fig. 6: Dice coefficient as a function of noise level for different INU values

Fig.6 illustrates white matter segmentation results compared to reference images. We notice that the curves first increase as noise in the unsegmented image increases. Our experimental results are due to the fact that the region growing phase with low noise becomes considerably discriminative (Eq.4). Low noise corresponds to a low standard deviation, which results in narrow comparison intervals. Assuming the initial region growing step aims to compute the characteristics of the region (region’s mean gray level and standard deviation), if an agent encounters only similar pixels during its random walk, it produces a final region growing predicate (Eq.4) that cannot assimilate any bordering pixels in the region that are affected by the partial volume effect, as illustrated in Fig.7b. Therefore, increasing noise increases the tolerance of the assimilation predicate, leading to segmentation where bordering pixels are well aggregated in the region (Fig.7d). However, when noise exceeds a certain threshold (5% for 0-20% INU and 3% for 40% INU), it affects the accuracy of the detected region borders. This is due to the increased standard deviation and alteration of the region’s mean gray levels, which are caused by the augmentation of the proportion of noise pixels inside the region. Changing the region’s mean gray levels results in wide comparison intervals (Eq.4). Moreover, noise combined with the partial volume effect causes the borders between regions to have lower contrast, making segmentation more complicated and decreasing segmentation accuracy. We also think this process starts earlier with a 40% INU level because the image becomes deteriorated (voxels belonging to the same tissues have disparate

gray levels), knowing that the latter is affected by a combination of three significant artefacts (partial volume effect, noise, and high INU).

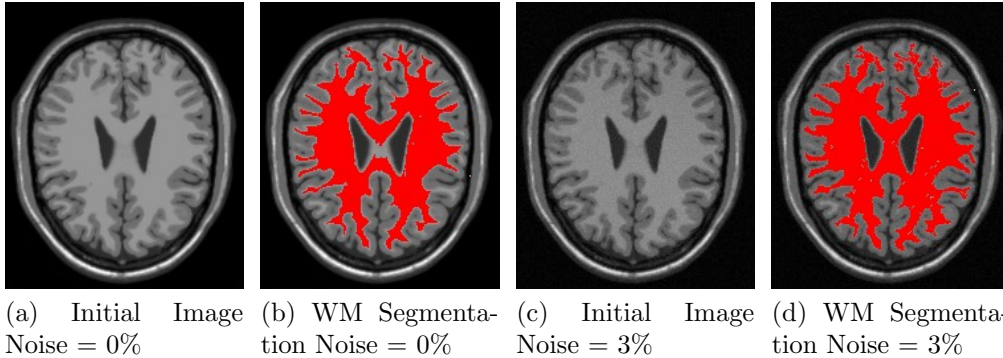


Fig. 7: White matter (WM) segmentation examples of a brain slice with 0% INU level for (7a) and (7b), and with 20% INU level for (7c) and (7d)

Experiments conducted with phantom MR images show the efficiency of our segmentation approach. Our approach can be used to segment an image and extract compact regions of interest, such as the white matter region. The results presented in Table 1 and Fig.6 show the robustness of MAMES as noise and INU increase. The Dice coefficient is always above 80%, even when $INU = 40\%$ and $noise = 9\%$.

These promising results led us to test the efficiency of MAMES with the laborious task of tumor segmentation in 3D MRI, for which the experimental results are introduced in the following section.

4.3. Experimental Results on 3D MR Tumoral Images

One of the main problems associated with the design of image segmentation methods is their evaluation process. This evaluation is generally based on comparing the experimental results with reference results produced manually by a human expert. However, achieving a set of manually segmented images (ideally done by several experts) is not an easy task, and it is very time-consuming (several hours to segment a single 3D MR image).

Existing work often uses small datasets produced by radiologists to evaluate their approaches. This procedure complicates the evaluation process as no shared data is available to compare segmentation methods. Thus, the BraTS challenge began in conjunction with the International Conference on Medical Image Computing (2012) to address the brain tumor segmentation issue.

The BraTS challenge ([70]) offers a useful environment for evaluating automatic segmentation approaches of tumor extraction in multi-modal 3D MR images. The BraTS dataset (BraTS2018) is composed only of pre-operative images acquired in four modalities (T1, T2, FLAIR, and T1 with contrast enhancement). It contains high-grade glioblastoma (HGG) and lower-grade glioma (LGG) manually segmented by experts. In the BraTS dataset, voxels in a reference image were divided into three different classes (labels), the enhanced tumor (label 4), peritumoral edema (label 2), and necrotic tumor core (label 1). A fourth label (label 3) was initially used to define non-enhancing tumor core, but it was eliminated afterward. This annotation was made by several domain experts and validated by experienced neuro-radiologists. Therefore, the MR images used in BraTS were acquired in different institutions with different equipment and protocols, making this dataset heterogeneous in terms of MRI rendering and quality (same tissue type can have different gray level intensities from one acquisition device to another).

The BraTS dataset takes the form of a set of folders, one folder for each human subject. Inside a folder, a multi-modal image is stored in five different files (four files for the MR image modalities and a file for the labeled reference).

To conduct our experiments, we used eight 3D images from the BraTS dataset. Considering that MAMES is designed for single modality images, we focus on the FLAIR modality as it offers desirable contrast between the tumoral area and the healthy tissues. The obtained tumor segmentation results are detailed in Table 2 and Fig.8. In the latter and in addition to the Dice coefficient, we include specificity (TNR), accuracy (ACC), precision (PPV), and sensitivity (TPR) as common metrics used for evaluating tumor segmentation.

$$TNR = \frac{TN}{TN + FP} \quad (7)$$

$$ACC = \frac{TP + TN}{TP + TN + FP + FN} \quad (8)$$

$$PPV = \frac{TP}{TP + FP} \quad (9)$$

$$TPR = \frac{TP}{TP + FN} \quad (10)$$

The quantitative evaluation presented in Table 2 and Fig.8 illustrate the

effectiveness of our approach for tumor segmentation in 3D MRI. The results of tumor segmentation exceed 80% for all eight volumes and an average of 86% Dice coefficient. These results are similar to those obtained by a segmentation expert when compared to the consensus obtained during development of the BraTS dataset [70].

3D Brain MRI	Eudema					Whole Tumor				
	TNR	ACC	PPV	TPR	Dice	TNR	ACC	PPV	TPR	Dice
MRI 1	99%	99%	99%	63%	77%	99%	99%	99%	76%	86%
MRI 2	99%	99%	72%	92%	81%	99%	99%	82%	88%	85%
MRI 3	99%	99%	88%	89%	88%	99%	99%	90%	90%	90%
MRI 4	99%	99%	98%	83%	89%	99%	99%	98%	80%	88%
MRI 5	99%	99%	99%	83%	90%	99%	99%	99%	75%	85%
MRI 6	99%	99%	99%	83%	90%	99%	99%	99%	75%	85%
MRI 7	99%	99%	91%	71%	80%	99%	99%	94%	76%	84%
MRI 8	99%	99%	87%	84%	85%	99%	99%	89%	84%	86%

Table 2: Specificity, accuracy, precision, sensitivity, and Dice coefficients for edema and whole tumor segmentation results using MAMES on the images in the BraTS dataset

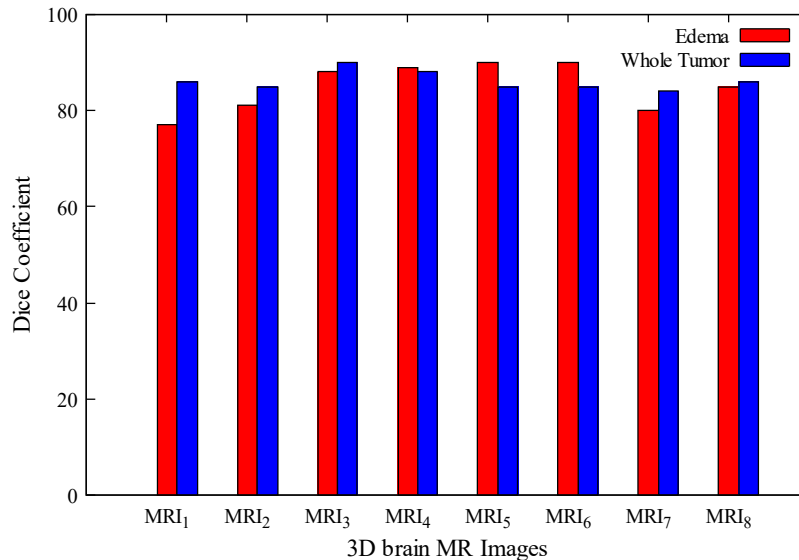


Fig. 8: Results for tumors segmentation in brain MR images from BraTS dataset

Tables 3 and 4 show results obtained by MAMES for segmentation of LGG and HGG tumors, respectively, in the axial, coronal, and sagittal planes. The first line shows different slices for the T1 modality, while the second line shows different slices for the FLAIR modality. From comparing these two modalities, we observe that FLAIR modality has higher contrast than the T1 modality; this is why the FLAIR modality was selected for tumor segmentation. The third line shows the final tumor segmentation results, which are highlighted in red in the T1 images. This illustration already makes it possible to judge the effectiveness of our approach. Additionally, rows four and five allow the obtained results to be compared with reference results.

When comparing the tumor segmentation results with reference results (rows four and five in Table 3 and Table 4), we notice some small undetected areas inside the segmented volume. This phenomenon is a common issue that occurs when the region growing method is used in medical images with textured regions [71]. In our experiments, those miss-detected regions are due to the inhomogeneity of the tumors. The tumors are composed of tissues (i.e., edema, necrotic core, and active tumor) that can have different intensities inside an MR image. Differentiation of those textures requires the use of multiple modalities (T1, T2, FLAIR, and T1e). Because our approach only uses the FLAIR modality to segment a tumor, resulting in these small undetected areas, this issue can be overcome by using some mathematical morphology operations.

A comparative evaluation of these results is presented in Table 5 and Fig.9. From the latter, we observe that our results are satisfactory when compared to some state-of-the-art approaches using the BraTS dataset [42]. We also highlight the fact that our approach uses only one modality (FLAIR) when most of the other presented methods use the four modalities provided in the BraTS dataset. Unfortunately, we could not compare our results to another multi-agent approach for 3D segmentation of brain tumors as this has not been published in another paper to the best of our knowledge.

From our different experiments, we conclude that the best segmentation results are obtained with an $\alpha \in [2, 2.5]$ for brain MR images.

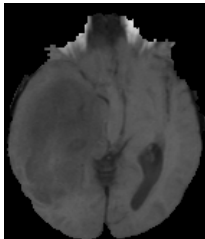
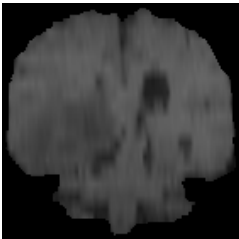
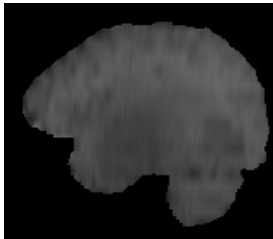
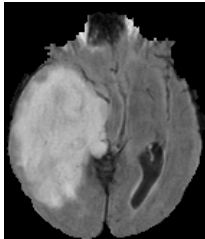
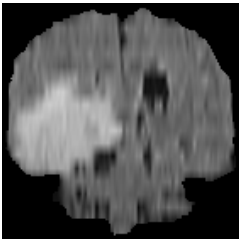
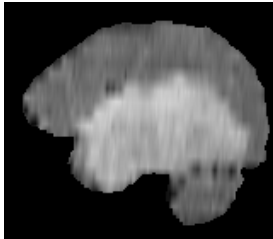
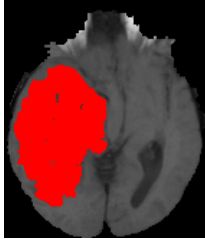
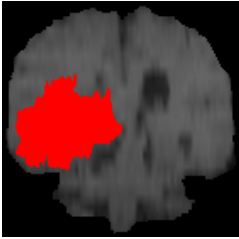
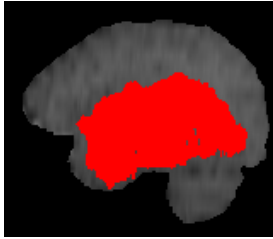
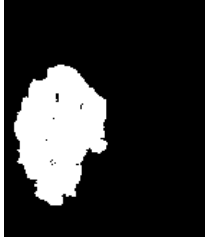
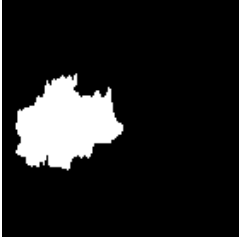




	Axial	Coronal	sagittal
T1			
FLAIR			
Tumor on T1			
Extracted Tumor			
Reference			

Table 3: LGG segmentation results in the axial, coronal, and sagittal planes

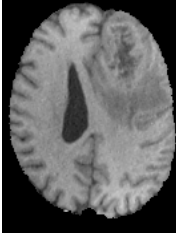
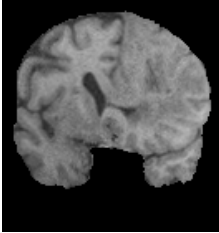
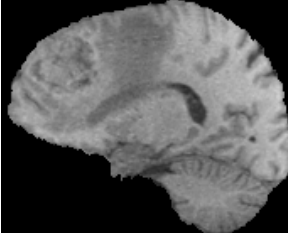
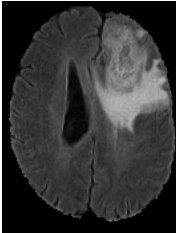

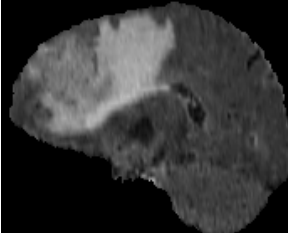
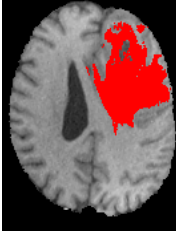
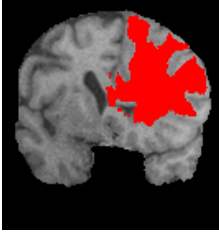
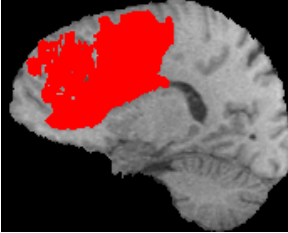

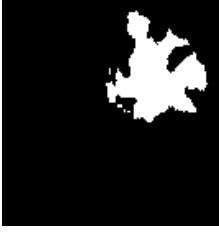




	Axial	Coronal	Sagittal
T1			
FLAIR			
Tumor on T1			
Extracted Tumor			
Reference			

Table 4: HGG segmentation results in the axial, coronal, and sagittal planes

Approach	Year	Method	Results (Dice)	N ^o of used modalities
Jiang [72]	2013	Graph - cut	84%	4
Havaei [73]	2014	KNN + MRF	85%	4
Pedoia [74]	2015	Competitive EM and graph cut	70%	1
Zabir [75]	2015	Region growing and level set evolution	81%	2
Kapás [76]	2015	Random forest	70%	4
Gupa [77]	2015	Intensity features of multimodality MRI	77%	4
Kapas [76]	2016	Binary decision trees and random forest technique	67%	4
Vishnu-varthanan [78]	2016	Self-organizing map + Fuzzy K means	92%	4
Pei [79]	2017	Cell density patterns/tumor growth modeling	82%	4
Dong [80]	2017	U-Net-based fully convolutional networks	86%	4
Havaei [81]	2017	Deep neural networks	88%	4
Chen [82]	2018	Densely connected 3D CNN	72%	4
Zhao [83]	2018	Fully convolutional neural networks+conditional random fields	87%	3
Ma [84]	2018	Random forests + multiscale patch-driven active contour	89%	4
Lim [85]	2018	Information theoretic rough sets	70%	4
MAMES	2020	Multi-agent cooperation using gradient thresholding and adaptive region growing	86%	1

Table 5: Comparative evaluation of whole tumor segmentation results with other state-of-the-art approaches

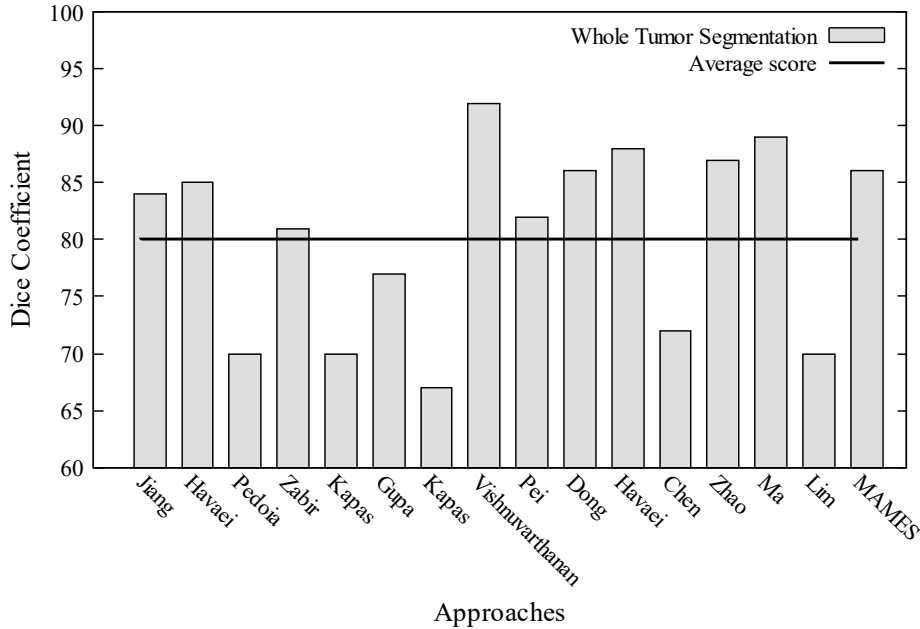


Fig. 9: Graphical representation of a comparative evaluation of whole tumor segmentation results with other state-of-the-art approaches

4.4. Result Analysis and Discussion

The results obtained with Phantom MR images from the brain web show that the MAMES results are reproducible despite the presence of artifacts, namely noise and INU. For any combination of noise and INU, the Dice coefficient remains above 85%, even in the worst case examined (Noise = 9%, INU = 40%). The obtained results were competitive with those of other methods published in the literature. However, and unlike most of the other methods that have obtained good scores, MAMES does not require any learning stage or manual segmentation of MR images. This is a major strong point of MAMES that allows fast MRI segmentation without referring to any pre-defined or acquired knowledge.

The robustness of MAMES regarding artifacts can be explained from two perspectives:

- MAMES is distributed and cooperative owing to its multi-agent design;
- The locality and stochasticity of treatments.

These two aspects allow segmentation of MR images that contain INU. The local treatments start randomly and the obtained local results are inte-

grated, given that the INU artifact can be neglected within small areas or volumes.

MAMES is a new approach derived from our method presented in [59], however, it introduces many new ideas and improvements. First of all, the approach presented in [59] uses only similarity detection with its multi-phase region growing method, while MAMES combines discontinuity detection and similarity detection in a sequential cooperative manner (see Section 3). This makes the experimental results of MAMES more accurate, despite an increase in noise. Unlike the approach presented in [59], MAMES does not need a “border refining and noise removal” step. Thanks to the voxel partitioning phase, the initial region growing process became more accurate for determining a regions’ parameters, making the final region growing step more efficient. Finally, MAMES was used on healthy and pathological 3D brain MR images without any pre-processing, where the approach in [59] involved segmentation of healthy brain MR images after a brain extraction pre-processing only in two dimensions using the Fsl tool [86]. This significant difference confirms the robustness of MAMES segmentation.

Using our equipment (described at the beginning of Section 4), the average segmentation time for 2D MR images is equal to 5 s, whereas 3D MR images require 2 min 20 s. Even if this duration seems substantial at first, especially for 3D segmentation, MAMES segments the entire image (not just the object of interest) in a cooperative manner, and our implementation does not use parallelization. Our current implementation uses pseudo-parallelism during execution, which explains the segmentation duration. Therefore, one direction of future research is implementation of a physically distributed version of MAMES, allowing the processing time to be decreased.

Experimental results on the BraTS database have shown the efficiency of MAMES for accurate segmentation of a brain tumor into its main parts, namely the entire tumor and the edema. The Dice coefficient results show that the proposed method provides segmentation accuracy that is close to the accuracy found with other cited methods, despite the fact that most of those methods are learning-based, and in some cases, require a massive training dataset, such as for deep learning-based methods.

Furthermore, no specific assumption about the image content has been considered. The only requirement is that the processed images be composed of visually separable regions. Thus, MAMES presents significant results with the extraction of compact areas as tumors or organs. However, MAMES faces difficulties when segmenting narrow structures. Therefore, our approach is

suitable for any type of medical images, such as CT scans and PET images, where the aim is to extract regions based on some homogeneity criterion. All the reviewed methods were designed for a specific type of image, thus they require important modifications if they are to be used with other types of images.

5. Conclusion

In this paper, we present a multi-agent approach, MAMES, for medical image segmentation. MAMES allows simultaneous detection of different regions without any input from the user related to the type of image, such as the number of regions, thresholds, or some characteristics that are pre-defined with a learning phase or a prior knowledge.

MAMES relies on a population of interactive agents that perform two main tasks: voxel partitioning for seed selection, and region growing for tissue extraction. After extracting all the regions, the agents start a coordinated merging process. For this part of the work, we were inspired by meta-heuristics to propose a distributed adaptation of the well-known simulated annealing algorithm, and adopt the concept of social welfare, where agents consider both individual rationality and social rationality.

MAMES was used to segment several brain MR images. The segmentation experiments validated its implementation and targeted characteristics performance, such as the segmentation quality. With only one modality, our approach offers similar and, in some cases, more accurate results than other approaches that use the four modalities provided by the BraTS dataset.

MAMES is a promising approach owing to the use of well-known segmentation techniques and a multi-agent architecture. One of our future research directions is to modify MAMES to consider several modalities in the same image simultaneously. We believe that those modalities would provide higher segmentation accuracy by producing a clearer distinction between different tissues composing the tumor.

We aim to focus on using our approach to segment other anatomical structures using other types of medical images (e.g., CT scans or functional MRI). Finally, segmentation could be tested with other region-extraction methods, such as machine-learning-based classification and clustering.

Acknowledgements

This research was supported by the Algerian General Directorate for Scientific Research and Technological Development.

References

- [1] M. Xu, W. Luk, P. Cutler, W. Digby, Local threshold for segmented attenuation correction of PET imaging of the thorax, *IEEE Transactions on Nuclear Science* 41 (4) (1994) 1532–1537.
- [2] R. Adams, L. Bischof, Seeded region growing, *IEEE Transactions on pattern analysis and machine intelligence* 16 (6) (1994) 641–647.
- [3] M. A. Kupinski, M. L. Giger, Automated seeded lesion segmentation on digital mammograms, *IEEE Transactions on medical imaging* 17 (4) (1998) 510–517.
- [4] K. Held, E. R. Kops, B. J. Krause, W. M. Wells, R. Kikinis, H.-W. Muller-Gartner, Markov random field segmentation of brain MR images, *IEEE transactions on medical imaging* 16 (6) (1997) 878–886.
- [5] T. McInerney, D. Terzopoulos, Deformable models in medical image analysis: a survey, *Medical image analysis* 1 (2) (1996) 91–108.
- [6] B. B. Avants, N. J. Tustison, M. Stauffer, G. Song, B. Wu, J. C. Gee, The Insight ToolKit image registration framework, *Frontiers in Neuroinformatics* 8 (2014) 1–13.
- [7] S. M. Smith, M. Jenkinson, M. W. Woolrich, C. F. Beckmann, T. E. Behrens, H. Johansen-Berg, P. R. Bannister, M. D. Luca, I. Drobnjak, D. E. Flitney, R. K. Niazy, J. Saunders, J. Vickers, Y. Zhang, N. D. Stefano, J. M. Brady, P. M. Matthews, Advances in functional and structural MR image analysis and implementation as FSL, *NeuroImage* 23 (2004) 208–219.
- [8] T. Zhou, S. Ruan, S. Canu, A review: Deep learning for medical image segmentation using multi-modality fusion, *Array* 2-3 (2019) 1–11.
- [9] M. H. Hesamian, W. Jia, X. He, P. Kennedy, Deep learning techniques for medical image segmentation: Achievements and challenges, *Journal of digital imaging* 32 (4) (2019) 582–596.

- [10] G. Weiss, *Multiagent Systems: A Modern Approach to Distributed Artificial Intelligence*, Intelligent Robotics and Autonomous Agents Series, MIT Press, 1999.
- [11] S. Chakraborty, S. Gupta, Medical Application Using Multi Agent System—A Literature Survey, *Journal of Engineering Research and Applications* 4 (2) (2014) 528–546.
- [12] N. Sharma, L. M. Aggarwal, et al., Automated medical image segmentation techniques, *Journal of medical physics* 35 (1) (2010) 3–14.
- [13] A. Elnakib, G. Gimel'farb, J. S. Suri, A. El-Baz, Medical image segmentation: A brief survey, in: *Multi Modality State-of-the-Art Medical Image Segmentation and Registration Methodologies*, Springer, 2011, pp. 1–39.
- [14] A. Albouy-Kissi, S. Cormier, F. Tranquart, Perfusion quantification of contrast-enhanced ultrasound images based on coherence enhancing diffusion and competitive clustering, in: *Image Processing (ICIP), 2012 19th IEEE International Conference on*, IEEE, 2012, pp. 2321–2324.
- [15] J. S. Duncan, N. Ayache, Medical image analysis: Progress over two decades and the challenges ahead, *IEEE transactions on pattern analysis and machine intelligence* 22 (1) (2000) 85–106.
- [16] C.-h. Chen, *Handbook of pattern recognition and computer vision*, World Scientific, 2015.
- [17] D. L. Pham, C. Xu, J. L. Prince, Current methods in medical image segmentation, *Annual review of biomedical engineering* 2 (1) (2000) 315–337.
- [18] J. Montagnat, H. Delingette, N. Ayache, A review of deformable surfaces: topology, geometry and deformation, *Image and vision computing* 19 (14) (2001) 1023–1040.
- [19] S. Angenent, E. Pichon, A. Tannenbaum, Mathematical methods in medical image processing, *Bulletin of the American mathematical society* 43 (3) (2006) 365–396.

- [20] S.-Y. Wan, W. E. Higgins, Symmetric region growing, *IEEE Transactions on Image processing* 12 (9) (2003) 1007–1015.
- [21] C.-H. Chuang, W.-N. Lie, Region growing based on extended gradient vector flow field model for multiple objects segmentation, in: *Proceedings 2001 International Conference on Image Processing (Cat. No. 01CH37205)*, Vol. 3, IEEE, 2001, pp. 74–77.
- [22] P. Anbeek, K. L. Vincken, G. S. Van Bochove, M. J. Van Osch, J. van der Grond, Probabilistic segmentation of brain tissue in MR imaging, *Neuroimage* 27 (4) (2005) 795–804.
- [23] K. Van Leemput, F. Maes, F. Bello, D. Vandermeulen, A. Colchester, P. Suetens, Automated segmentation of MS lesions from multi-channel MR images, in: *International Conference on Medical Image Computing and Computer-Assisted Intervention*, Springer, 1999, pp. 11–21.
- [24] Y. Zhang, M. Brady, S. Smith, Segmentation of brain MR images through a hidden Markov random field model and the expectation-maximization algorithm, *IEEE transactions on medical imaging* 20 (1) (2001) 45–57.
- [25] K. Van Leemput, F. Maes, D. Vandermeulen, P. Suetens, A unifying framework for partial volume segmentation of brain MR images, *IEEE transactions on medical imaging* 22 (1) (2003) 105–119.
- [26] D. L. Pham, Robust fuzzy segmentation of magnetic resonance images, in: *Proceedings 14th IEEE Symposium on Computer-Based Medical Systems. CBMS 2001*, IEEE, 2001, pp. 127–131.
- [27] S. Chen, D. Zhang, Robust image segmentation using FCM with spatial constraints based on new kernel-induced distance measure, *IEEE Transactions on Systems, Man, and Cybernetics, Part B (Cybernetics)* 34 (4) (2004) 1907–1916.
- [28] W. Bai, W. Shi, C. Ledig, D. Rueckert, Multi-atlas segmentation with augmented features for cardiac MR images, *Medical image analysis* 19 (1) (2015) 98–109.
- [29] T. Rohlfing, R. Brandt, R. Menzel, C. R. Maurer, Evaluation of atlas selection strategies for atlas-based image segmentation with application

- to confocal microscopy images of bee brains, *NeuroImage* 21 (4) (2004) 1428–1442.
- [30] D. Zhang, Q. Guo, G. Wu, D. Shen, Sparse patch-based label fusion for multi-atlas segmentation, in: *International Workshop on Multimodal Brain Image Analysis (MBIA 2012)*, Lecture Notes in Computer Science, Heidelberg, Vol. 7509, Springer, 2012, pp. 94–102.
 - [31] G. Yang, J. Gu, Y. Chen, W. Liu, L. Tang, H. Shu, C. Toumoulin, Automatic kidney segmentation in CT images based on multi-atlas image registration, in: *2014 36th Annual International Conference of the IEEE Engineering in Medicine and Biology Society, IEEE*, 2014, pp. 5538–5541.
 - [32] P. Rajendran, M. Madheswaran, Hybrid medical image classification using association rule mining with decision tree algorithm, *Journal of computing* 2 (1) (2010).
 - [33] X. Du, Y. Li, D. Yao, A support vector machine based algorithm for magnetic resonance image segmentation, in: *2008 Fourth International Conference on Natural Computation*, Vol. 3, IEEE, 2008, pp. 49–53.
 - [34] C. Lindner, S. Thiagarajah, J. M. Wilkinson, G. A. Wallis, T. F. Cootes, arcOGEN Consortium, et al., Fully automatic segmentation of the proximal femur using random forest regression voting, *IEEE transactions on medical imaging* 32 (8) (2013) 1462–1472.
 - [35] G. Litjens, T. Kooi, B. E. Bejnordi, A. A. A. Setio, F. Ciompi, M. Ghafoorian, J. A. Van Der Laak, B. Van Ginneken, C. I. Sánchez, A survey on deep learning in medical image analysis, *Medical image analysis* 42 (2017) 60–88.
 - [36] A. Işın, C. Direkoğlu, M. Şah, Review of MRI-based brain tumor image segmentation using deep learning methods, *Procedia Computer Science* 102 (2016) 317–324.
 - [37] M. Angulakshmi, G. Lakshmi Priya, Automated brain tumour segmentation techniques—A review, *International Journal of Imaging Systems and Technology* 27 (1) (2017) 66–77.

- [38] H. P. A. Tjahyaningtijas, Brain tumor image segmentation in MRI image, in: IOP Conference Series: Materials Science and Engineering, Vol. 336, IOP Publishing, 2018, p. 012012.
- [39] M. Zawish, A. A. Siyal, S. H. Shahani, A. Z. Junejo, A. Khalil, Brain Tumor Segmentation through Region-based, Supervised and Unsupervised Learning Methods: A Literature Survey, *Journal of Biomedical Engineering and Medical Imaging* 6 (2) (2019) 08–26.
- [40] H. A. Jalab, A. M. Hasan, Magnetic Resonance Imaging Segmentation Techniques of Brain Tumors: A Review, *Archives of Neuroscience* 6 (Brain Mapping) (2019) 1–7.
- [41] N. Gordillo, E. Montseny, P. Sobrevilla, State of the art survey on MRI brain tumor segmentation, *Magnetic resonance imaging* 31 (8) (2013) 1426–1438.
- [42] M. Hameurlaine, A. Moussaoui, Survey of Brain Tumor Segmentation Techniques on Magnetic Resonance Imaging, *Nano Biomed. Eng* 11 (2) (2019) 178–191.
- [43] S. Bakas, M. Reyes, A. Jakab, S. Bauer, M. Rempfler, A. Crimi, R. T. Shinohara, C. Berger, S. M. Ha, M. Rozycki, M. Prastawa, E. Alberts, J. Lipková, J. B. Freymann, J. S. Kirby, M. Bilello, H. M. Fathallah-Shaykh, R. Wiest, J. Kirschke, B. Wiestler, R. R. Colen, A. Kotrotsou, P. LaMontagne, D. S. Marcus, M. Milchenko, A. Nazeri, M. Weber, A. Mahajan, U. Baid, D. Kwon, M. Agarwal, M. Alam, A. Albiol, A. Albiol, A. Varghese, T. A. Tuan, T. Arbel, A. Avery, P. B., S. Banerjee, T. Batchelder, K. N. Batmanghelich, E. Battistella, M. Bendszus, E. Benson, J. Bernal, G. Biros, M. Cabezas, S. Chandra, Y. Chang, et al., Identifying the Best Machine Learning Algorithms for Brain Tumor Segmentation, Progression Assessment, and Overall Survival Prediction in the BRATS Challenge, *CoRR* abs/1811.02629 (2018).
- [44] F. Altaf, S. Islam, N. Akhtar, N. K. Janjua, Going Deep in Medical Image Analysis: Concepts, Methods, Challenges and Future Directions, *IEEE Access* 7 (2019) 99540–99572.
- [45] N. Benamrane, S. Nassane, Medical image segmentation by a multi-agent system approach, in: *German Conference on Multiagent System Technologies*, Springer, 2007, pp. 49–60.

- [46] R. Mohammed, A. Said, An Adaptative Multi-agent System Approach for Image Segmentation, *International Journal of Computer Applications* 51 (12) (2012).
- [47] E. Duchesnay, J.-J. Montois, Y. Jacquélet, Cooperative agents society organized as an irregular pyramid: A mammography segmentation application, *Pattern Recognition Letters* 24 (14) (2003) 2435–2445.
- [48] K. E. Melkemi, S. Foufou, Fuzzy distributed genetic approaches for image segmentation, *CIT. Journal of Computing and Information Technology* 18 (3) (2010) 221–231.
- [49] R. Moussa, M. M. Beurton-Aimar, P. Desbarats, On the use of social agents for image segmentation, in: *International Conference on complex systems and applications (iccsa 2009)*, Le Havre, France, 2009, pp. 1–7.
- [50] S. Djemame, M. Nekkache, M. Batouche, A Multi-Agent System for Image Segmentation A Bio-Inpired Approach, in: *Proceedings of the Third international conference on Innovation and Information and Communication Technology*, British Computer Society, 2009, pp. 17–17.
- [51] J. Liu, Y. Y. Tang, Adaptive image segmentation with distributed behavior-based agents, *IEEE Transactions on Pattern Analysis and Machine Intelligence* 21 (6) (1999) 544–551.
- [52] N. Richard, M. Dojat, C. Garbay, Distributed Markovian segmentation: Application to MR brain scans, *Pattern Recognition* 40 (12) (2007) 3467–3480.
- [53] S. Kumar, A. Lenin Fred, S. Muthukumar, H. Ajay Kumar, P. Sebastian Varghese, A voyage on medical image segmentation algorithms, *JA voyage on medical image segmentation algorithms Special Issue: S75-S87* (2018) 75–87.
- [54] J. Fan, G. Zeng, M. Body, M.-S. Hacid, Seeded region growing: an extensive and comparative study, *Pattern recognition letters* 26 (8) (2005) 1139–1156.
- [55] N. Richard, M. Dojat, C. Garbay, Automated segmentation of human brain MR images using a multi-agent approach, *Artificial Intelligence in Medicine* 30 (2) (2004) 153–176.

- [56] M. Chitsaz, C.-S. Woo, Medical image segmentation using a multi-agent system approach, *Int. Arab J. Inf. Technol.* 10 (3) (2013) 222–229.
- [57] R. Haroun, F. Boumghar, S. Hassas, L. Hamami, A massive multi-agent system for brain MRI segmentation, in: *International Workshop on Massively Multiagent Systems*, Springer, 2004, pp. 174–186.
- [58] C. Pereira, D. Veiga, J. Mahdjoub, Z. Guessoum, L. Gonçalves, M. Ferreira, J. Monteiro, Using a multi-agent system approach for microaneurysm detection in fundus images, *Artificial intelligence in medicine* 60 (3) (2014) 179–188.
- [59] M. T. Bennai, Z. Guessoum, M. Smaine, S. Cormier, M. Mezghiche, Towards a Generic Multi-Agent Approach for Medical Image Processing, in: *The 20th International Conference on Principles and Practice of Multi-Agent Systems (PRIMA 2017)*., 2017, pp. 198–211.
- [60] J. Toriwaki, H. Yoshida, *Fundamentals of three-dimensional digital image processing*, Springer Science & Business Media, 2009.
- [61] R. Pohle, K. D. Toennies, Segmentation of medical images using adaptive region growing, in: *Medical Imaging 2001*, International Society for Optics and Photonics, 2001, pp. 1337–1346.
- [62] Smith, Reid G, The Contract Net Protocol: High-Level Communication and Control in a Distributed Problem Solver, *IEEE Transactions on Computers* C-29 (12) (1980) 1104–1113.
- [63] R. G. Smith, The contract net protocol: High-level communication and control in a distributed problem solver, *IEEE Transactions on computers* C-29 (12) (1980) 1104–1113.
- [64] S. Bouveret, J. Lang, Efficiency and envy-freeness in fair division of indivisible goods: Logical representation and complexity, *Journal of Artificial Intelligence Research* 32 (2008) 525–564.
- [65] D. Bouyssou, T. Marchant, P. Perny, Social Choice Theory and Multicriteria Decision Aiding, in: *Decision-making Process Concepts and Methods*, ISTE / Wiley, 2009, pp. 741–770.

- [66] U. Endriss, N. Maudet, Welfare engineering in multiagent systems, in: International Workshop on Engineering Societies in the Agents World IV. ESAW 2003. Lecture Notes in Computer Science, Vol. 3071, Springer, 2003, pp. 93–106.
- [67] S. Bouveret, M. Lemaunefredtre, Computing Leximin-Optimal Solutions in Constraint Networks, *Artif. Intell.* 173 (2) (2009) 343–364.
- [68] A. P. Zijdenbos, B. M. Dawant, R. A. Margolin, A. C. Palmer, Morphometric analysis of white matter lesions in MR images: method and validation, *IEEE transactions on medical imaging* 13 (4) (1994) 716–724.
- [69] D. L. Collins, A. P. Zijdenbos, V. Kollokian, J. G. Sled, N. J. Kabani, C. J. Holmes, A. C. Evans, Design and construction of a realistic digital brain phantom, *IEEE transactions on medical imaging* 17 (3) (1998) 463–468.
- [70] B. H. Menze, A. Jakab, S. Bauer, J. Kalpathy-Cramer, K. Farahani, J. Kirby, Y. Burren, N. Porz, J. Slotboom, R. Wiest, L. Lanczi, E. Gerstner, M. Weber, T. Arbel, B. B. Avants, N. Ayache, P. Buendia, D. L. Collins, N. Cordier, J. J. Corso, A. Criminisi, T. Das, H. Delingette, C. Demiralp, C. R. Durst, M. Dojat, S. Doyle, J. Festa, F. Forbes, E. Geremia, B. Glocker, P. Golland, X. Guo, A. Hamamci, K. M. Iftekharruddin, R. Jena, N. M. John, E. Konukoglu, D. Lashkari, J. A. Mariz, R. Meier, S. Pereira, D. Precup, S. J. Price, T. R. Raviv, S. M. S. Reza, M. Ryan, D. Sarikaya, L. Schwartz, H. Shin, J. Shotton, C. A. Silva, N. Sousa, N. K. Subbanna, G. Szekely, T. J. Taylor, O. M. Thomas, N. J. Tustison, G. Unal, F. Vasseur, M. Wintermark, D. H. Ye, L. Zhao, B. Zhao, D. Zikic, M. Prastawa, M. Reyes, K. Van Leemput, The Multimodal Brain Tumor Image Segmentation Benchmark (BRATS), *IEEE Transactions on Medical Imaging* 34 (10) (2015) 1993–2024.
- [71] X. Zhang, X. Li, Y. Feng, A medical image segmentation algorithm based on bi-directional region growing, *Optik* 126 (20) (2015) 2398–2404.
- [72] J. Jiang, Y. Wu, M. Huang, W. Yang, W. Chen, Q. Feng, 3d brain tumor segmentation in multimodal mr images based on learning population-

- and patient-specific feature sets, *Computerized Medical Imaging and Graphics* 37 (7-8) (2013) 512–521.
- [73] M. Havaei, P.-M. Jodoin, H. Larochelle, Efficient interactive brain tumor segmentation as within-brain kNN classification, in: *2014 22nd International Conference on Pattern Recognition, IEEE*, 2014, pp. 556–561.
 - [74] V. Pedoia, S. Balbi, E. Binaghi, Fully automatic brain tumor segmentation by using competitive em and graph cut, in: *International Conference on Image Analysis and Processing, Springer*, 2015, pp. 568–578.
 - [75] I. Zabir, S. Paul, M. A. Rayhan, T. Sarker, S. A. Fattah, C. Shahnaz, Automatic brain tumor detection and segmentation from multi-modal MRI images based on region growing and level set evolution, in: *2015 IEEE International WIE Conference on Electrical and Computer Engineering (WIECON-ECE)*, 2015, pp. 503–506.
 - [76] Z. Kapás, L. Lefkovits, L. Szilágyi, Automatic detection and segmentation of brain tumor using random forest approach, in: *International Conference on Modeling Decisions for Artificial Intelligence (MDAI 2016). Lecture Notes in Computer Science, Vol. 9880, Springer*, 2016, pp. 301–312.
 - [77] M. Gupta, B. P. Rao, V. Rajagopalan, A. Das, C. Kesavadas, Volumetric segmentation of brain tumor based on intensity features of multimodality magnetic resonance imaging, in: *2015 International Conference on Computer, Communication and Control (IC4), IEEE*, 2015, pp. 1–6.
 - [78] G. Vishnuvarthanan, M. P. Rajasekaran, P. Subbaraj, A. Vishnuvarthanan, An unsupervised learning method with a clustering approach for tumor identification and tissue segmentation in magnetic resonance brain images, *Applied Soft Computing* 38 (2016) 190–212.
 - [79] L. Pei, S. M. S. Reza, W. Li, C. Davatzikos, K. M. Iftekharuddin, Improved brain tumor segmentation by utilizing tumor growth model in longitudinal brain MRI, in: *Medical Imaging 2017: Computer-Aided Diagnosis, Vol. 10134, International Society for Optics and Photonics, SPIE*, 2017, pp. 666 – 674.
 - [80] H. Dong, G. Yang, F. Liu, Y. Mo, Y. Guo, Automatic brain tumor detection and segmentation using u-net based fully convolutional networks, in:

- annual conference on medical image understanding and analysis (MIUA 2017). Communications in Computer and Information Science, Vol. 723, Springer, 2017, pp. 506–517.
- [81] M. Havaei, A. Davy, D. Warde-Farley, A. Biard, A. Courville, Y. Bengio, C. Pal, P.-M. Jodoin, H. Larochelle, Brain tumor segmentation with deep neural networks, *Medical image analysis* 35 (2017) 18–31.
 - [82] L. Chen, Y. Wu, A. M. DSouza, A. Z. Abidin, A. Wismüller, C. Xu, MRI tumor segmentation with densely connected 3D CNN, in: *Medical Imaging 2018: Image Processing*, Vol. 10574, International Society for Optics and Photonics, SPIE, 2018, pp. 357–364.
 - [83] X. Zhao, Y. Wu, G. Song, Z. Li, Y. Zhang, Y. Fan, A deep learning model integrating FCNNs and CRFs for brain tumor segmentation, *Medical image analysis* 43 (2018) 98–111.
 - [84] C. Ma, G. Luo, K. Wang, Concatenated and connected random forests with multiscale patch driven active contour model for automated brain tumor segmentation of MR images, *IEEE transactions on medical imaging* 37 (8) (2018) 1943–1954.
 - [85] K. Y. Lim, R. Mandava, A multi-phase semi-automatic approach for multisequence brain tumor image segmentation, *Expert Systems with Applications* 112 (2018) 288–300.
 - [86] M. Jenkinson, M. Pechaud, S. Smith, BET2: MR-based estimation of brain, skull and scalp surfaces, in: *Eleventh annual meeting of the organization for human brain mapping*, Vol. 17, Toronto., 2005, p. 167.